Science Press

ARTICLE

Effect of WC-17Co Powder Density on Coating Mechanical Properties and Residual Stress

Liu Yankuan,   Yang Sinan,   Wang Zhiping

Tianjin Key Laboratory of Civil Aircraft Airworthiness and Maintenance, Civil Aviation University of China, Tianjin 300300, China

Abstract: Three kinds of WC-17Co powders with different densities were selected as starting material, and a coating with 0.3 mm in thickness was prepared by high velocity oxygen fuel (HVOF) method. The porosity of the three coatings was analyzed by SEM, the Knoop hardness and Young's modulus of the coatings were measured by indentation method. At the same time, the residual stress of the WC-17Co coating prepared by powders with different densities was measured by layer-stripping method. Results show that the porosity level of the coatings increases with increasing WC-17Co powder density, while the Knoop hardness and Young's modulus of the coatings decrease with the increase of powder density. The residual stress existing in the WC-17Co coating appears as compressive stress, which increases with the increase of the coating depth, and then decreases rapidly near the coating-substrate interface. The maximum residual stresses of the coatings deposited with powder density of 11.52, 12.86 and 13.49 g·cm^{-3} are −798, −986 and −1120 MPa, respectively.

Key words: HVOF; WC-17Co; powder density; mechanical properties; residual stress

High velocity oxygen fuel (HVOF) spraying technology refers to the use of combustible gas fuel (such as hydrogen, propane or propylene) or combustible liquid fuel (such as aviation kerosene) mixed with oxygen (or compressed air) as a combustion gas, which is then ignited and burned in a high-pressure combustion chamber. After that, the violently burned and expanded combustion gas is constrained and compressed by the nozzle to form a supersonic flame stream. The powder material to be sprayed is fed in by the powder feeding gas (such as nitrogen) in an axial or radial direction along the combustion chamber, and is ejected after being heated and accelerated in the flame[1,2]. Tungsten carbide (WC) coating prepared by HVOF method is used to strengthen the surface of important parts of the aircraft, which can enhance the stability and work efficiency of the parts, and its better wear resistance and corrosion resistance make it successfully replace the hard chromium electroplating[2-5].

HVOF spraying technology is mainly used for the preparation of cermet coatings, and the relatively high speed and low temperature of WC powder particles during spraying are the two most important characteristics. The high in-flight speed of the powder particles brings a high impact energy onto the matrix. While the relatively low temperature of the powder particles will inhibit the phase transition and oxidative decomposition of the material, so the HVOF deposited coating has high density and high bonding strength, and is easy to form a high-quality coating[6-8].

The residual stress of the coating prepared by the HVOF method is a key factor leading to the early failure of the coating. It has an important influence on the stress control, debonding analysis and service lifetime prediction of the components[9]. Residual stress as a kind of internal stress refers to a state of stress that remains in the component and maintains its own balance due to uneven volume changes and deformation when the various factors that produce stress no longer exist[10]. The failure of WC coating is largely determined by the residual stress inside the coating. The process of preparing WC coating by HVOF spraying technology has experienced impact, deposition, and sudden temperature changes. At the same time, there are differences

in thermophysical and mechanical properties between the sprayed material and the base material. These factors lead to the generation of residual stress in the process of preparing the coating by HVOF. The reasons for this mainly include impact stress, thermal stress and quenching stress. In the HVOF spraying technology, the surface of the coating, the bonding between the coatings layers, and the interface between coating and substrate are the areas where the structural defects are concentrated, and are also the original areas where the residual stress causes the coating to failure. Normally, the main types of coating failure due to residual stress include cracking[11,12], delamination[13,14] and warping[15].

In the studies on the residual stress of WC coatings, most scholars and researchers adopted finite element simulation analysis methods, X-ray diffraction methods and other research methods. Gui et al[16] studied the effects of five factors, including oxygen flow rate, kerosene flow rate, powder feed rate, spraying distance and spray gun moving speed, on the residual stress of WC-Co-Cr coating during HVOF spraying process. The results show that the residual stress in the coating is expressed as a residual compressive stress, and the value of the compressive stress is affected by the substrate material, particle flying speed, temperature, and substrate surface temperature. At the same time, spraying distance has the greatest influence on the residual stress of the coating among the five factors, followed by the oxygen flow rate and the kerosene flow rate. In the short-distance spraying process, the high-temperature and high-speed WC-Co-Cr particles produce higher impact stress and thermal stress on the surface of the substrate, which make the coating obtain a larger residual compressive stress. Stokes et al[17] combined finite element method and experimental method to study the residual stress of WC-Co coating prepared by HVOF method. Results show that the deviation between the finite element simulation and the experimental measurement results is only 14%. Meanwhile, the finite element test results show that the thickness of the coating is the dominant factor that affects the residual stress. A coating with a larger thickness will lead to a larger residual stress value. Smith et al[18] compared and analyzed the micro-morphology and internal residual stress of three different carbide coatings: Cr3C2-NiCr, WC-Co and WC-CoCr. While Greying et al[19] researched the residual stress in the thickness direction of the WC-17Co coating, but

there is little research on the residual stress of the WC-17Co coating prepared by different powder types of WC material.

It can be seen that there is little research on the performance and properties of the tungsten carbide coating deposited by different WC powder particles. Our group previously studied the effect of WC-17Co powder size on the mechanical properties of the coating [20]. On this basis, the influence of powder density differences on coating performance and residual stress is further studied. Firstly, three WC-17Co powders with different densities were selected as starting materials, and the coatings with the same thickness were prepared by HVOF method. Secondly, the mechanical properties of the three different coatings were compared and analyzed. Finally, the residual stress in the thickness direction of different types of WC-17Co coatings was tested and studied by the layer-stripping method. The effect of WC-17Co powder density on the mechanical properties and internal residual stress of the coating was revealed.

1 Experiment

1.1 Test materials

In this experiment, the substrate material was In718 nickel-based alloy, and the specimen size was 15 mm×15 mm×3 mm. The physical properties of the substrate material are as follows: Young's modulus 204 GPa and Poisson's ratio 0.3.

The spray material was WC-17Co powder produced by Metco, United States. Three kinds of powder particles (type-1, type-2, and type-3) with the same particle size and different densities were selected through the sieve shaker. The diameter of the powder was 10~40 μm, and the densities of type-1, type-2 and type-3 were tested as 11.52, 12.86 and 13.49 g·cm^{-3}, respectively by Quarrz AU-300PM powder metallurgy density detector, fabricated by Hangzhou Jinmai Instrument Co., Ltd, China. The micromorphology of the three kinds of powders are shown in Fig.1 by a scanning electron microscope (SEM). It can be seen that the WC-17Co powder particles are approximately spherical or ellipsoidal, and the particle size is quasi-uniform.

1.2 Coating preparation

The JP5000 liquid fuel-oxygen HVOF system produced by TAFA, United States was applied during the coating fabrication process. In order to ensure accurate and stable control of the spraying distance and speed, the 2400M six-axis
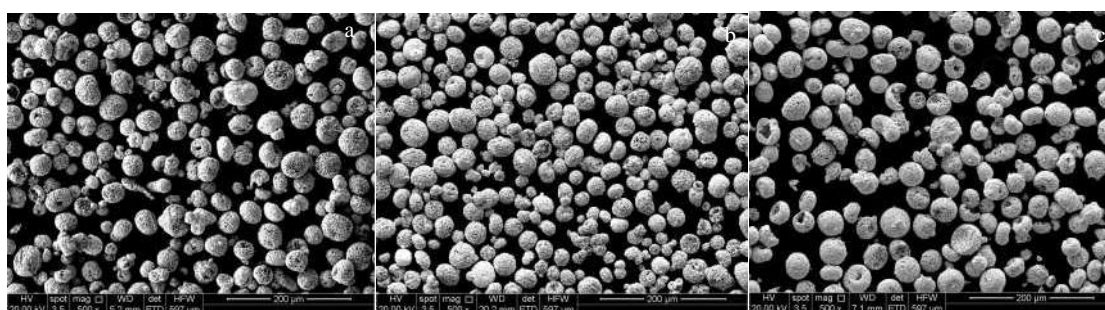

Fig.1   Micro-morphologies of WC-17Co powders with different densities: (a) type-1, (b) type-2, and (c) type-3

automatic manipulator produced by American ABB Company was used to control the spraying process. The thickness of the WC-17Co coating was 0.3 mm.

1.3 Micro-morphology analysis and mechanical property test of coating

The Quanta FEG250 field emission scanning electron microscope (SEM) produced by Czech FEI Company was used to observe the micro-morphology and the "OLYCIA LEXT" software produced by Olympus Japan was applied to analyze the density and porosity of the coatings prepared by WC-17Co powder particles with different densities.

The Knoop microhardness and Young's modulus of the coating were measured by the HVS-1000 microhardness tester[21]. The load was 2.94 N with a loading time of 20 s, the indenter was a pyramidal diamond, as shown in Fig.2, and the angles between the top two flutes was α and β, which are 172.5° and 130°, respectively. The Knoop hardness value was the average of 10 indentation test points.

The formula for calculating Knoop hardness (HK) is:

$$\text{HK} = 1.451\frac{F}{a} \tag{1}$$

where F=2.94 N, and a is the length of the long diagonal of the indentation.

The formula for calculating Young's modulus (E) is:

$$E = \frac{\alpha\text{HK}}{\dfrac{b}{a} - \dfrac{b'}{a'}} \tag{2}$$

where α is a constant 0.45; b/a is the ratio of the short diagonal to the long diagonal of the indentation, which is 1/7.11; b'/a' is the ratio of the short diagonal to the long diagonal of the indentation. The Young's modulus is also the average value of 10 indentation test points.

1.4 Residual stress of coating

The residual stress distributed along the thickness of the coating was measured and calculated by layer-stripping method in this experiment[19]. H-610 adhesive was used to paste strain gauges on the three different types of specimens as required. Layers of coating were stripped in a wet forming surface grinder, the stripping thickness for each layer was 0.02 mm, and the stripping time was 25. Thus the total stripping thickness was 0.5 mm (0.3 mm of coating and 0.2 mm of substrate). Each time of stripping should be paused for 10~15 min, in order to read a stable and constant value displayed by the dynamic resistance strain gauge. This test was carried out at room temperature. The strain energy inside the coating will be released by grindin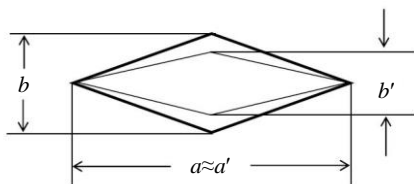g and removing the coating layers. At the same time, resistance strain gauges were used to successively measure the overall strain change of the specimen, while the balance of force and moment, and the stress-strain characteristics of the material were mainly used to determine the distribution and magnitude of the residual stress in the specimen[22].

Fig.3 is a schematic illustrating the above stripping method. F_x is the force applied in the x direction of the coating, and the force and moment acted on the substrate are related to F_x through the balance of force-moment. The thickness of the substrate is H, the thickness of the coating removed each time is h, and the thickness of the remaining coating is h'. The length and width of the specimen are recorded as b_x and b_y, respectively, noting that b_y is not shown in the figure. The Young's modulus and Poisson's ratio of the coating are E_c and v_c, respectively. And the corresponding Young's modulus and Poisson's ratio of the substrate are E_b and v_b, respectively.

It should be pointed out that the strain gauge is attached to the surface of the specimen opposite to the coating, and it records the strain change of the surface. Therefore, after each time of stripping, the actual strain change on the specimen is equal to the opposite value of the obtained strain data.

1.4.1   Relationship between residual stress and strain

Set the center plane of the specimen as the reference plane (z=0). As the stripping test proceeds, the distribution of strain along the direction of thickness is a linear function of z, as presented in Eq.(3).

$$\begin{aligned} \varepsilon_x &= \varepsilon_{x0} + K_x z \\ \varepsilon_y &= \varepsilon_{y0} + K_y z \end{aligned} \tag{3}$$

where ε_x and ε_y are the strain distribution along the thickness of the specimen; ε_{x0} and ε_{y0} represent the strain of the middle plane (z=0), K_x and K_y are the plane curvatures of the middle plane (z=0) in the x and y directions, respectively. The stress-strain equation for the isotropic plane stress behavior of the coating and the substrate is as follows:

$$\begin{bmatrix} \sigma_x \\ \sigma_y \end{bmatrix} = E'\begin{bmatrix} 1 & v \\ v & 1 \end{bmatrix}\begin{bmatrix} \varepsilon_x \\ \varepsilon_y \end{bmatrix} \tag{4}$$

where σ_x and σ_y are the stresses in the x and y directions, respectively; v represents either the Poisson's ratio of the coating or the Poisson's ratio of the substrate, which can be expressed as v_c and v_b, respectively. And for E', it can be represented as $E'_c=E_c/(1-v_{c2})$ and $E'_b=E_b/(1-v_{b2})$ for the coating

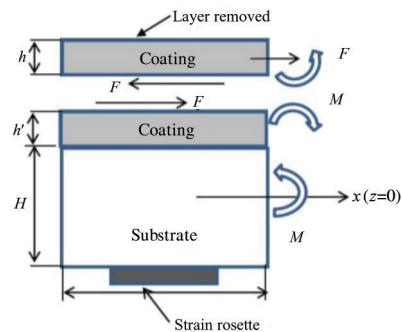Fig.2   Schematic diagram of Knoop indentation

Fig.3   Schematic diagram of peeling method

and the substrate, respectively.

1.4.2 Resultant force and resultant moment

F_x' and F_y' are defined as the force per unit length, and M_x' and M_y' are the moment per unit length. The resultant force and resultant moment can be easily calculated, as shown in Eq.(5).

$$F_x' = \frac{F_x}{b_x}, F_y' = \frac{F_y}{b_y}$$
$$M_x' = \frac{M_x}{b_x}, M_y' = \frac{M_y}{b_y}$$
(5)

The resultant force and the resultant moment can be expressed in the form of a matrix and they can be related to the stress, as shown in Eq.(6):

$$\begin{bmatrix} F_x' \\ F_y' \end{bmatrix} = \int_{-(H+h')/2}^{(H+h')/2} \begin{bmatrix} \sigma_x \\ \sigma_y \end{bmatrix} dz$$
$$\begin{bmatrix} M_x' \\ M_y' \end{bmatrix} = \int_{-(H+h')/2}^{(H+h')/2} \begin{bmatrix} \sigma_x \\ \sigma_y \end{bmatrix} z dz$$
(6)

Substituting Eq. (3) and Eq. (4) into Eq. (6), we can get Eq.(7):

$$\begin{bmatrix} F_x' \\ F_y' \\ M_x' \\ M_y' \end{bmatrix} = \begin{bmatrix} A_{11} & A_{12} & B_{11} & B_{12} \\ A_{12} & A_{22} & B_{12} & B_{22} \\ B_{11} & B_{12} & D_{11} & D_{12} \\ B_{12} & B_{22} & D_{12} & D_{22} \end{bmatrix} \begin{bmatrix} \varepsilon_{x0} \\ \varepsilon_{y0} \\ K_x \\ K_y \end{bmatrix}$$
(7)

Among them:

$$A_{11} = A_{22} = E_b'H + E_c'h'$$
$$A_{12} = v_b E_b'H + v_c E_c'h'$$
$$B_{11} = B_{22} = (E_c' - E_b')Hh'/2$$
$$B_{12} = (v_c E_c' - v_b E_b')Hh'/2$$
$$D_{11} = D_{22} = \frac{E_b'}{12}H(H^2 + 3h'^2) + \frac{E_c'}{12}h'(h'^2 + 3H^2)$$
$$D_{12} = \frac{v_b E_b'}{12}H(H^2 + 3h'^2) + \frac{v_c E_c'}{12}h'(h'^2 + 3H^2)$$
(8)

1.4.3 Calculation equation of layer-stripping method

The relationship between the strain change $\Delta\varepsilon_{xG}$, $\Delta\varepsilon_{yG}$ and ε_{x0}, ε_{y0} on the side where the strain gauge is attached after the coating is stripped off can be expressed as:

$$\varepsilon_{x0} = \Delta\varepsilon_{xG} + K_x(H + h')/2$$
$$\varepsilon_{y0} = \Delta\varepsilon_{yG} + K_y(H + h')/2$$
(9)

Substituting Eq.(9) into Eq.(7) to obtain Eq.(10):

$$\begin{bmatrix} F_x' \\ F_y' \\ M_x' \\ M_y' \end{bmatrix} = \begin{bmatrix} A_{11} & A_{12} & B_{11} & B_{12} \\ A_{12} & A_{22} & B_{12} & B_{22} \\ B_{11} & B_{12} & D_{11} & D_{12} \\ B_{12} & B_{22} & D_{12} & D_{22} \end{bmatrix} \left(\begin{bmatrix} \Delta\varepsilon_{xG} \\ \Delta\varepsilon_{yG} \\ 0 \\ 0 \end{bmatrix} + \begin{bmatrix} K_x(H+h')/2 \\ K_y(H+h')/2 \\ K_x \\ K_y \end{bmatrix} \right)$$
(10)

At the same time, Eq. (11) expresses the relationship between the resultant force and the resultant moment applied on the residual specimen and the stress of the removed coating:

$$\begin{bmatrix} F_x' \\ F_y' \\ M_x' \\ M_y' \end{bmatrix} = - \begin{bmatrix} \sigma_{xL}h \\ \sigma_{yL}h \\ \sigma_{xL}h(H + h' + h)/2 \\ \sigma_{yL}h(H + h' + h)/2 \end{bmatrix}$$
(11)

where σ_{xL} and σ_{yL} are the coating stresses that are stripped off.

It can be seen that four equations involving four unknowns σ_{xL}, σ_{yL}, K_x, K_y can be obtained by Eq.(10) and Eq.(11), and the above formulas can be combined to obtain Eq.(12):

$$\begin{bmatrix} h & 0 & A_{11}T + B_{11} & A_{12}T + B_{12} \\ 0 & h & A_{12}T + B_{12} & A_{22}T + B_{22} \\ T'h & 0 & B_{11}T + D_{11} & B_{12}T + D_{12} \\ 0 & T'h & B_{12}T + D_{12} & B_{22}T + D_{22} \end{bmatrix} \begin{bmatrix} \sigma_{xL}h \\ \sigma_{yL}h \\ K_x \\ K_y \end{bmatrix}$$
$$= - \begin{bmatrix} A_{11} & A_{12} \\ A_{12} & A_{22} \\ B_{11} & B_{12} \\ B_{12} & B_{22} \end{bmatrix} \begin{bmatrix} \Delta\varepsilon_{xG} \\ \Delta\varepsilon_{yG} \end{bmatrix}$$
(12)

where $T=(H+h')/2$ and $T'=(H+h'+h)/2$.

Solving Eq.(12) can get the residual stress σ_{xL} and σ_{yL} of the stripped off coating, and the curvature change K_x and K_y of the specimen.

Finally, according to the test data, the Young's modulus value and the as-known Poisson's ratio of the different types of coatings measured by the indentation method, the residual stress distribution of the coating along the thickness direction can be calculated by Eq.(12).

2 Results and Discussion

2.1 Effect of powder density on mechanical properties of WC-17Co coating

Fig. 4 shows the porosity levels of the HVOF sprayed coating observed and analyzed by SEM, which are prepared by three WC-17Co powders with different densities. The
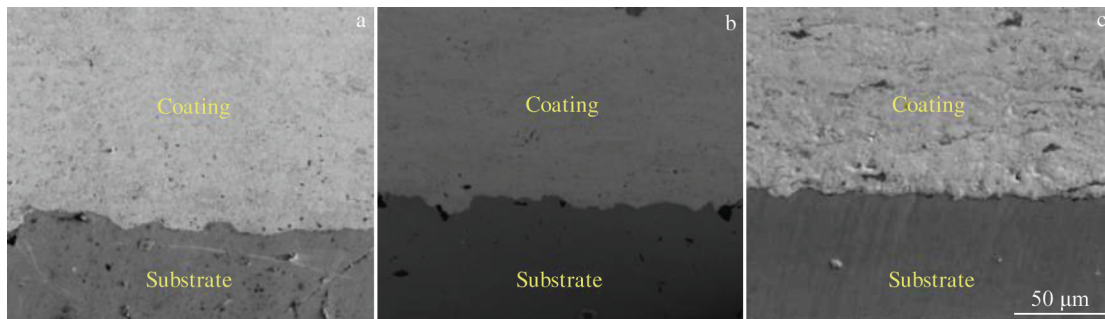

Fig.4   SEM images of coatings deposited with different powder densities: (a) type-1, (b) type-2, and (c) type-3

porosity (μ) of the three coatings are $(0.59\pm0.07)\%$, $(0.81\pm 0.09)\%$ and $(1.02\pm0.12)\%$ for type-1, type-2 and type-3 coating, respectively (Table 1). It can be seen that the coating porosity increases with increasing the particle density. That is because as the density of type-1 powder is the smallest, the melting status of particles are the best during spraying process as the heat can be transferred more rapidly inside the particle, so the degree of flattening of the particles during deposition process will be high, the filling effect between the particles is better, and the corresponding coating has a low porosity and a high density. On the contrary, as the type-3 powder has the highest density, a poor degree of melting during spraying will occur due to the slower heat transfer process inside the particle, resulting in low degree of flattening when impacting onto the surface of substrate, therefore a high porosity and a low density of coating will be obtained[20].

The Knoop hardness indentation loaded on the three types of coatings are presented in Fig.5. Then the values of Knoop hardness and Young's modulus of three coatings were measured by Eq.(1) and Eq.(2), respectively. The test results are shown in Table 1 and Fig.6.

It can be seen that the density (i.e. the porosity level) of the coating affects the basic mechanical properties of the coating, such as the hardness and Young's modulus. High-density coatings have higher hardness and Young's modulus, while low-density coatings have lower hardness and Young's modulus.

The powder with low particle density (type-1) can transfer the heat more rapidly by itself during in-flight process, and its melting status before impacting the substrate is better, so the coating will have a higher density, then the hardness and Young's modulus of the coating will be higher as well. On the contrary, there may be areas that are not fully melted before impacting the substrate for the powder with high density, as it will take longer time for heat transfer compared to low density

particle. We can see clearly from Fig.7 that there are unmelted WC-17Co particles in the coating. So the coating formed by this kind of powder is a non-uniform and porous coating (also shown in Fig.7), resulting in lower density, lower hardness and also lower Young's modulus.

2.2 Effect of powder density on residual stress of WC-17Co coating

Fig.8 shows the residual stress distribution in the thickness direction of the coatings prepared by three types of WC-17Co powders. The results show that the interior of the matrix of the three specimens all appears as tensile stress, while at the surface of the substrate and the entire coating all appear as compressive stress. This is because the powder has a high in-flight speed during HVOF spraying process, which is usually 700~800 m/s[20].

In the thickness direction of the coating, the residual compressive stress gradually increases with the increase of the stripped thickness, and reaches the maximum near the interface between coating and substrate. This is because as discussed before, residual stress is mainly generated under the action of impact stress, thermal stress and quenching stress. The particles have high kinetic and thermal energy when they hit the substrate or the anterior layer of coating, and they are prone to generate large impact stress and thermal stress. For the position close to the substrate, the thickness is deep, and the number of impacts experienced during the coating preparation process is also greater, so the accumulated residual compressive stress value is the largest.

Then the value of residual compressive stress at the interface between coating and substrate decreases rapidly, and even the residual stress on the substrate appears as tensile stress. This can be explained by the fact that the In718 nickel based alloy is a homogeneous and dense material with good toughness, so it has better deformation and heat transfer ability after impacted by WC-17Co powders, so the compressive stress can be effectively released.

Fig.9 shows the maximum residual stress and the depth position of the coating prepared by WC-17Co powders with different densities. It can be seen that the maximum value of the compressive residual stress of the coating increases with the increase of the powder density, and the position of the maximum value of the residual compressive stress in the thickness direction of the coating increases with increasing the

Table 1　Porosity, Knoop hardness and Young's modulus of WC-17Co coatings deposited with different powder densities

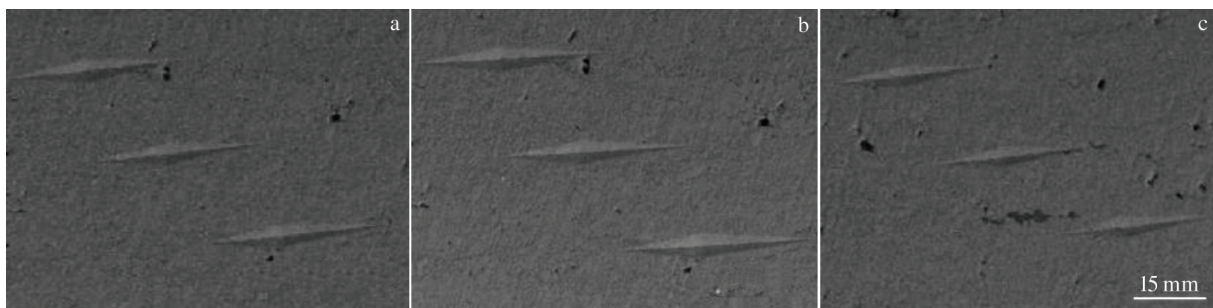| Property	Type-1	Type-2	Type-3
μ/%	0.59 ± 0.07	0.81 ± 0.09	1.02 ± 0.12
HK/$\times10$ MPa	1268 ± 45	1103 ± 33	1054 ± 51
E/GPa	350 ± 21	305 ± 26	291 ± 19

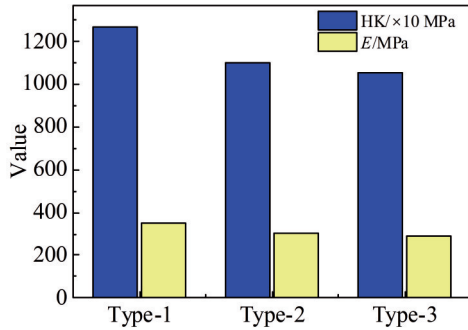Fig.5　Knoop indentations in different WC-17Co coatings: (a) type-1, (b) type-2, and (c) type-3

Fig.6 Knoop hardness and Young's modulus of coatings prepared with different densities of WC-17Co powders
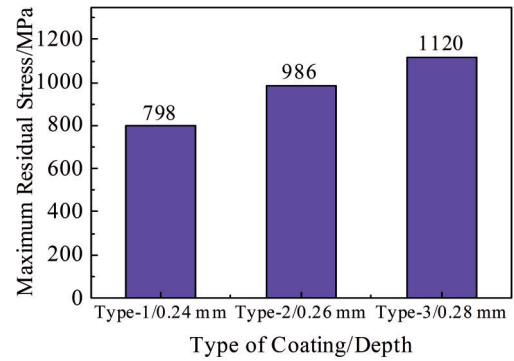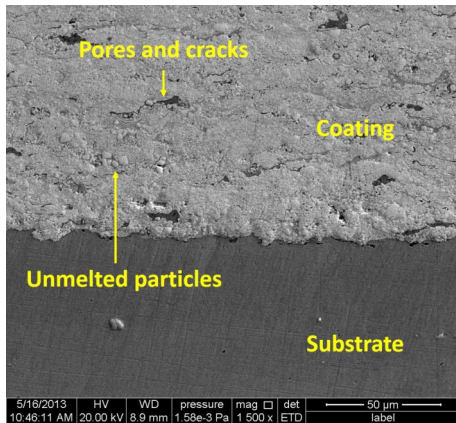

Fig.7 Unmelted area and porous area found in type-3 coating
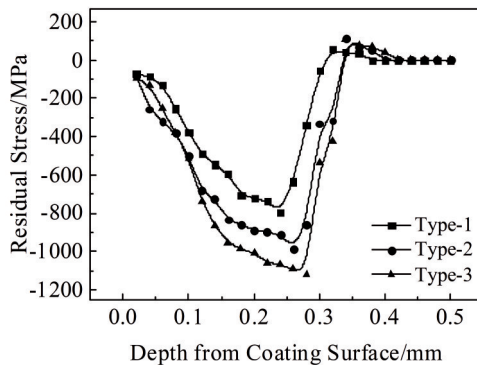

Fig.8 Residual stress distribution of coatings prepared by WC-17Co powders with different densities

powder density.

(1) Type-1 powder has the smallest density, and its maximum residual compressive stress is −798 MPa, which appears at a distance of 0.24 mm from the coating surface.

(2) Type-2 powder has moderate particle density, and its maximum residual compressive stress is −986 MPa, which appears at a distance of 0.26 mm from the coating surface.

(3) Type-3 powder has the highest particle density, and its maximum residual compressive stress is −1120 MPa, which appears at a distance of 0.28 mm away from the coating

Fig.9 Maximum residual stress and depth of coatings prepared by WC-17Co powders with different densities

surface.

It can be seen that the kinetic energy of the particles will be converted to plastic deformation energy and elastic deformation energy after impacting the substrate, and then accumulated as residual compressive stress, while particles with higher density have greater in-flight kinetic energy and stronger impact on the substrate, so the maximum internal residual stress will be also greater. At the same time, the position where the maximum residual stress appears is closer to the substrate (further from the coating surface).

3 Conclusions

1) The porosity of the coating is positively correlated with the density of the WC-17Co powder: the porosity of the coating processed with powder densities of 11.52 g·cm^{-3} (type-1), 12.86 g·cm^{-3} (type-2) and 13.49 g·cm^{-3} (type-3) is 0.59%, 0.81% and 1.02%, respectively.

2) Both Knoop hardness and Young's modulus of the coating decrease with increasing the density of WC-17Co powder. The Knoop hardness (HK) of type-1, type-2 and type-3 coatings is 12 680, 11 030 and 10 540 MPa, respectively, and the Young's modulus is 350, 305 and 291 GPa, respectively.

3) The residual stress existing in the WC-17Co coating appears as compressive stress, and it is distributed along the thickness of the coating. The stress value increases with the thickness of the coating (from surface to in-depth), and decreases rapidly near the interface between coating and substrate.

4) The maximum residual compressive stress of the WC-17Co coating increases with the increase of WC-17Co powder density. The maximum residual stresses of coatings of type-1, type-2 and type-3 are −798, −986 and −1120 MPa, respectively, which appear at 0.24, 0.26 and 0.28 mm below the coating surface, respectively.

5) In engineering applications, high-hardness coatings have higher wear resistance, while low-hardness coatings have better bending resistance. Therefore, the mechanical properties such as coating's hardness and Young's modulus cannot fully explain the criteria of coating quality. In actual applications, the process should be optimized according to

different applications and requirements of the coating to determine the best preparation plan.

References

1 Wielage B, Wank A, Pokhmurska H *et al. Surface & Coatings Technology*[J], 2006, 201(5): 2032

2 Wang Yongbing, Liu Xiang, Qi Wenjun *et al. Electroplating & Finishing*[J], 2007, 26(7): 52

3 Fu Junbo, Zhou Shikui. *Failure Analysis and Prevention*[J], 2006, 1(2): 61

4 Chen Lishun, Zhang Bin, Cai Yuangang. *Aeronautical Manufacturing Technology*[J], 2011, 11: 34

5 Li Changjiu. *Thermal Spray Technology*[J], 2018, 10(4): 1

6 Kanno A, Takagi K, Arai M. *Surface & Coatings Technology*[J], 2020, 394: 125 881

7 Yao H L, Zhang M X, Yang C *et al. Ceramics International*[J], 2020, 46(11): 19 431

8 Chen Q Y, Fu W, Du D M *et al. Rare Metal Materials and Engineering*[J], 2019, 48(11): 3680 (in Chinese)

9 Brindley W J, Whittenberger J D. *Material Science Engineering*[J], 1993, 163(1): 33

10 Zhou Yu. *Material Analysis Method*[M]. Beijing: China Machine Press, 2000: 61 (in Chinese)

11 Teixeira V. *Vacuum*[J], 2002, 64: 393

12 Jiang Wei, Xu Binshi, Wang Haidou. *Heat Treatment of Metals* [J], 2007, 32(1): 25

13 Lemaitre J. *Handbook of Material Behavior Models*[M]. New York: Academic Press, 2001: 582

14 Choi S R, Hutchinson J W, Evans A G. *Mechanics of Materials* [J], 1999: 431

15 Lee S L, Windover D. *Surface & Coatings Technology*[J], 1998, 108-109: 65

16 Gui M, Eybel R, Asselin B *et al. Journal of Materials Engineering and Performance*[J], 2012, 21(10): 2090

17 Stokes J, Looney L. *Journal of Materials Engineering and Performance*[J], 2009, 18(1): 21

18 Smith G M, Gildersleeve E J, Luo X T *et al. Surface & Coatings Technology*[J], 2020, 387: 125 536

19 Greying D J, Rybicki E F, Shadley J R. *Journal of Thermal Spray Technology*[J], 1994, 3(4): 379

20 Liu Yankuan, Wang Zhiping, Ding Kunying. *Surface Technology* [J], 2016, 45(6): 76

21 Lima R S, Krüger S E, Lamouche G *et al. Journal of Thermal Spray Technology*[J], 2005, 14(1): 52

22 Zoei M S, Sadeghi M H, Salehi M. *Surface & Coatings Technology*[J], 2016(307): 886

WC-17Co粉末密度对涂层力学性能及残余应力的影响

刘延宽，杨斯楠，王志平

(中国民航大学 天津市民用航空器适航与维修重点实验室，天津 300300)

摘 要：选取3种不同密度的WC-17Co粉末，采用超音速火焰喷涂法制备厚度为0.3 mm的涂层。通过扫描电镜观察分析了3种涂层的孔隙率，采用压痕法测量了涂层的努氏硬度与弹性模量，同时采用剥层法对不同密度粉末制备的WC-17Co涂层残余应力进行了测试与计算。结果表明，涂层孔隙率随WC-17Co粉末密度的增大而增大，涂层的努氏硬度、弹性模量均随WC-17Co粉末密度的增大而减小。WC-17Co涂层内部存在的残余应力表现为压应力，且应力值随涂层厚度的增大而增加，在临近涂层-基体界面处迅速减小。涂层残余压应力最大值随WC-17Co粉末密度的增大而增加：粉末密度为11.52、12.86、13.49 g·cm⁻³所制备的涂层残余应力最大值分别为−798、−986和−1120 MPa。

关键词：超音速火焰喷涂；WC-17Co；粉末密度；力学性能；残余应力

作者简介：刘延宽，男，1988年生，博士，中国民航大学，天津 300300，电话：022-24092114，E-mail：liuyankuan314@163.com